# Top-down ion mobility/mass spectrometry reveals enzyme specificity: Separation and sequencing of isomeric proteoforms

Francis Berthias[1], Nurgül Bilgin[2], Jasmin Mecinović[2], Ole N. Jensen[1*]

[1]Department of Biochemistry and Molecular Biology, [2]Department of Physics, Chemistry and Pharmacy, University of Southern Denmark, Campusvej 55, DK-5230 Odense M, Denmark.

## ABSTRACT

Enzymatic catalysis is one of the fundamental processes that drives the dynamic landscape of post-translational modifications (PTMs), expanding the structural and functional diversity of proteins. Here, we assessed enzyme specificity using a top-down ion mobility spectrometry (IMS) and tandem mass spectrometry (MS/MS) workflow. We successfully applied trapped IMS (TIMS) to investigate site-specific N-$\varepsilon$-acetylation of lysine residues of full-length histone H4 catalyzed by histone lysine acetyltransferase KAT8. We demonstrate that KAT8 exhibits a preference for N-$\varepsilon$-actylation of residue K16, while also installing N-$\varepsilon$-acetyl groups on residues K5 and K8 as the first degree of acetylation. Achieving TIMS resolving power values of up to 300, we fully separated mono-acetylated regioisomers (H4K5ac, H4K8ac, and H4K16ac). Each of these regioisomers produce unique MS/MS fragment ions, enabling estimation of their individual mobility distributions and the exact localization of the N-$\varepsilon$-acetylation sites. This study highlights the potential of top-down TIMS-MS/MS for conducting enzymatic assays at the intact protein level and, more generally, for separation and identification of isomeric proteoforms and precise PTM localization.

## 1. INTRODUCTION

Protein post-translational modifications (PTMs) significantly enhance the functional diversity of proteins, expanding proteome complexity beyond what is encoded in the genome[1]. Enzymatic catalysis is one of the fundamental processes that drives the dynamic landscape of PTM by addition or removal of functional groups from specific residues of proteins. PTMs occur in response to cellular developmental programs, growth signals and physiological requirements[2], and are dysregulated in many pathological conditions[3,4]. Consequently, PTM enzymes (a.k.a PTM writers, readers, erasers) that precisely regulate PTMs are potential targets for drug development[5]. Profiling such enzymes to understand and determine their substrate specificity is valuable through assays in which PTMs of proteins, or peptide substrates, are quantitatively and directly measured[6].

PTMs play such an important role for histone proteins that they presumably constitute an epigenetic code (the "histone code" hypothesis)[7]. PTMs regulate the genome during cell fate determination and development and are implicated in disease-related cellular processes, including cancers, neurological disorders or autoimmune diseases[8,9]. With more than 400 known PTMs to date and enzymes responsible for over 200 kinds of modifications of protein substrates[10,11], the vast number of potential PTM combinations along with the reversible nature of many of them, gives rise to an abundant number of proteoforms. These proteoforms includes isobaric (near-identical mass) and isomeric (same mass) proteoforms, all of biological importance[12]. Indeed, the same modification occurring at different sites (PTM positional isomers or regioisomers) can be associated to different biological activities and regulatory behaviors, such as acetylation of histone H4 lysine residues[13,14] or trimethylation of histone H3 lysine residues[13,15]. Mapping, quantifying, understanding and even predicting the role PTM patterns represent a forefront challenge of biology[16].

To achieve unambiguous identification and in-depth characterization of proteoforms, proteins must be analyzed at the intact level. Top-down mass spectrometry (MS)-based analysis examines intact proteins without enzymatic proteolysis, preserving PTM connectivity[17,18]. Although isomeric proteoforms can be identified based on unique MS/MS fragments ions pairs, in practice MS-based proteomics encounters challenges when dealing with complex sample containing more than two isomers and potential isobaric species, resulting in chimeric MS/MS spectra. High resolution MS can resolve isobaric species to some extent, depending on the

resolution performance on the mass analyzer, but it must be use in concert with separation technique prior the mass selection to reduce the spectral complexity. While liquid chromatography (LC) offers high separation capability at the peptide-level, its performance diminishes for larger species (>2–3 kDa). Chromatographic resolution may be achieved to distinguish and quantify some proteoforms with advanced and complex chromatographic protocols[19,20], nevertheless isomeric proteoforms for the most part coelute, thus hampering the detection of their presence or precise quantification. Therefore, complementary and/or alternative separation methods are needed.

Incorporating ion mobility spectrometry (IMS) into the top-down-MS workflow enhances dynamic range and sequence coverage by reducing the spectral complexity[21–23]. IMS rapidly (ms-sec) separates gas-phase molecular ions based on their three-dimensional structure, exploiting the fact that ions of different sizes, shapes, and charges travel at different average velocities in an inert gas under the influence of an electric field (E)[24]. In addition, the estimation of ion-neutral collision cross section (CCS) by some IMS analyzer provides valuable structural information[25]. Due to very similar drift behavior of isomeric proteoforms which only differ between each other by minute structural differences (~1% and less of CCS difference), ultimate resolving power is of higher priority. Recent advanced IMS technologies[26] such as Trapped IMS (TIMS)[27], cyclic IMS (cIM)[28], and Structures for Lossless Ion Manipulation (SLIM)[29] offer high-resolution capabilities, reaching resolving powers of up to 300-400 and even more than 1000 in specific cases[30]. Such high resolution IMS analyzers successfully enabled separation for long isomeric peptides (~5 kDa)[31] and very recently on small proteins (~11 kDa)[32].

We assessed Trapped IMS coupled with tandem mass spectrometry for the separation and identification of intact histone H4 decorated with one and several N-$\varepsilon$-acetyl groups at distinct lysine residues. Among the many protein acetylation marks found in chromatin, histone H4 lysine 16 acetylation (H4K16ac) is particularly notable for its ability to decompact the chromatin structure.[33] H4K16 is known to be the primary catalytic site of KAT8 acetyltransferase, and it has recently been reported to also acetylate two additional lysine residues, namely, H4K5 and H4K8.[34] Given its potential to acetylate multiple lysine residues, we performed *in vitro* KAT8 acetylation assays on intact histone H4 and we demonstrate the potential of top-down IMS-MS/MS to characterize isomeric proteoforms and profiling the enzyme specificity at the intact protein level.

## 2. METHODOLOGY

Figure 1 presents a schematic overview of the methodology employed.

**Acetylation reaction.** Unmodified intact histone H4 from *Xenopus laevis* (identical to human histone H4) and human KAT8 acetyltransferase were expressed in-house following reported protocols.[35,36] Cofactor acetyl coenzyme A (AcCoA) was purchased from Sigma-Aldrich.

The KAT8 enzyme was incubated with histone H4 an AcCoA under the following conditions: 2 µM KAT8, 100 µM H4, 300 µM AcCoA; in reaction buffer: 50 mM HEPES, 0.1 mM EDTA, 1 mM DTT, pH = 8.0. in a final volume of 100 µL and shaken at 37 °C. KAT8 activity was stopped with the addition of 10% TFA in Milli-Q water after 3 hours. Due to incompatibility with ESI conditions, a buffer exchange to Milli-Q water was performed by ultrafiltration (centrifugation at 7000 g) using a membrane with a molecular weight cutoff of 3 kDa (Vivaspin). The sample was diluted to a final concentration of 3 µM, measured using a nanodrop spectrophotometer (NanoPhotometer N60-Touch, Implen), for subsequent IMS-MS/MS analysis in a methanol/water/formic acid solution with ratios of 50/49/1, respectively. In addition, a control samples consisting of unmodified H4 dissolved directly in the ESI solvent was prepared.

**TIMS Separation principle**. Experiments were performed on a timsTOF Pro2 hybrid Q-TOF tandem mass spectrometer (Bruker Daltonics). The fundamental concept underlying TIMS separation, which has been widely described[27,37–39], involves reversing the traditional drift-tube IMS analyzer approach. Instead of propelling gas-phase ions through a stationary gas with an electric field, ions are entrained in a drift gas flow under the influence of an electric field oriented in the opposite direction of their propagation. Thus, ions with different ion mobilities are trapped at different equilibrium position in the TIMS tunnel corresponding to where the forward drag force imposed by the drift gas is counterbalanced by the deceleration force imposed by E. Ions thus trapped are then sequentially eluted into mass spectrometer by ramping E down at a define scan rate (Sr).

**TIMS settings and calibration.** Samples were infused via a Captive-Spray ESI emitter at a flow rate of 250 nL/min using a nanoElute LC system (Bruker Daltonics) in direct infusion with an ESI voltage of 1.3 kV. Mass-over-charge ratio was calibrated by utilizing the ESI-L low

concentration tunemix (Agilent). Since TIMS does not directly measure absolute mobility coefficient values (K), a priori calibration using species with known mobility is necessary. We used three species from the aforementioned tune mix. These singly charged species have mass-over-charge ratio values of 622.0288, 922.0085 and 1221.9906 with corresponding $1/K_0$ values 0.9915, 1.1986 and 1.3934 V·s/cm², where $K_0$ represents the reduced ion mobility coefficient. The ion-neutral collision cross sections with $N_2$ gas (CCS) are calculated via the Mason-Schamp equation (eq. 1) and reference mobility values from calibrants 202.96, 243.64 and 282.20 Å², respectively:

$$CCS = \frac{3}{16}\sqrt{\frac{2\pi}{\mu k_b T}}\frac{ze}{NK} \quad (1)$$

where e is elementary charge, $k_b$ is the Boltzmann constant, T is the temperature, N is the number density of the drift gas, and $\mu$ is the reduced mass of the molecular ion and gas molecule. Since K varies with the pressure (P) and T, for comparison between experiments and IMS analyzers, K is corrected to reduced mobility $K_0$ at standard temperature and pressure ($T_0$ and $P_0$, respectively) with $K_0 = K(PT_0)/(P_0T)$.

**TIMS resolving power enhancement.** The TIMS resolving power, $R_{IMS}$, is determined by calculating the centroid of a peak in an IMS spectrum divided by its full width at half maximum (FWHM), $R_{IMS} = CCS/FWHM$. Several key parameters were adapted to maximize the resolving power of the TIMS analyzer: a high pressure of 3.4 mbar in the TIMS entrance and a slow ramping time ($t_{ramp}$) of 1.3 sec were employed. These values were chosen based on the fact that $R_{IMS}$ depends linearly on the drift gas velocity and the inverse fourth root of Sr (inversely proportional to $t_{ramp}$)[27]. The use of a faster gas flow requires a stronger electric field, increasing the ion heating which can potentially reduce conformational multiplicity through annealing. The DC bias between accumulation and TIMS region ("Δt6" in the timsTOF control software) was set to its maximum value (200 V). Increasing Δt6 accelerates ions before TIMS analysis thus enhancing collision energies and potentially narrowing TIMS peaks.

**Tandem mass spectrometry.** Collision-induced dissociation (CID) spectra in $N_2$ gas were recorded for specific *m/z* values of interest with an isolation window of 2 unit. Excitation voltages of 32 V and 29 V were applied for charge states 16+ and 17+, respectively. The presented MS/MS data represents an average of spectra over ~5 minutes), which is in the expected order of magnitude of chromatographic base peak width for histone H4 using reverse phase LC.[20].

**Data analysis.** Deconvolution of MS spectra presented in Figure 2b were obtained using UNIDEC.[40] Data analysis and characteristic b-fragment ions were extracted from raw files using DataAnalysis software (Bruker Daltonics) with a mass tolerance of ±10 ppm. Table S1 provides the experimental monoisotopic *m/z*, the theoretical monoisotopic mass, and the corresponding error of fragment ions. Fragments of type b were favored over the y-fragments due to lower mass and charge states, which eliminated isobaric interference.

## 3. RESULTS AND DISCUSSION

The primary objective is to evaluate the *in vitro* activity and selectivity of the KAT8 enzyme by determining the different degrees of acetylation produced. Figure 2a presents the heatmap of $1/K_0$ values as a function of *m/z* after incubating H4 with KAT8 and AcCoA for 3 hours. The resulting mass and deconvoluted mass spectra Figure 2b (black), along with the deconvoluted mass spectra of the control sample (teal). In absence of KAT8, only the unmodified histone is detected and additional peaks at higher masses values are observed in the presence of KAT8. These peaks match with the expected masses for H4 at three different degrees of acetylation (H4Kac1, H4Kac2, and H4Kac3), indicated by theoretical average mass in grey annotation. In this condition, the acetylation reaction yield is approximately 80%, and the most abundant degree of acetylation is mono-acetylation with an abundance of 40 % compared to 30% and 10% for di- and tri-acetylation, respectively.

Due to the addition of acetyl groups on lysine residues, the availability of protonation sites on the protein decreases, resulting in estimated average charge states of 15.4, 15.3, 15.1, and 14.8 for unmodified H4, H4Kac1, H4Kac2, and H4Kac3, respectively (cf. Figure S1). We could expect a reduction of one charge per acetylated lysine, but at a low pH, we can hypothesis that there is possibility for other protonation sites among the lysine, arginine, and histidine residues, despite the reduction of the number of available lysines.

Figure 2c shows inverse mobility/CCS distribution of the higher charge states using Sr = 23 V/s of charge states 16+ and 17+. These two charge states strike a balance between precursor intensity and resolving power. Indeed, higher charge state often exhibits the best TIMS separation and a higher $R_{IMS}$, given that $R_{IMS}$ is proportional to $(z)^{1/2}$. The inverse mobility distributions for the other the charge states are presented in Figure S2 using lower resolution (Sr = 64 V/s), and Figure S3 shows a comparison with the control sample, which

indicate the absence of degradation of unmodified H4 during the acetylation reaction and buffer exchange processes.

In summary, *in vitro* acetylation reaction in the presence of KAT8 produces three degrees of acetylation of H4, implying means that three lysine residues are targeted by the enzyme. Inverse mobility distributions of the unmodified H4 exhibit multiple contributions for each charge state, indicating the presence of several conformers.

The next step focuses on the determination the number of isomers for each degree of acetylation, *i.e.,* identifying the different acetylation site, using TIMS for gas-phase separation and MS/MS(CID) for sequencing and identification. In Figure 3, the top panel displays the sum of all the detected fragments from H4Kac1 at charge state 16+ (black curve), which is equivalent to the $1/K_0$ distribution of the precursor ion. Figure 3b shows b-fragment ions ($b_6^{1+}$ and $b_7^{1+}$) exhibiting a +42 Da mass difference demonstrating the presence of an acetyl group on K5 (red curve). As fragmentation occurs after mobility analysis, fragments retain the same IMS profile as their parent ions. Therefore, the red curve corresponds to the specific inverse mobility distribution of H4K5ac.

Similarly, all b-fragment ions containing an acetylation produced by fragmentation occurring between lysine residues 8 and 12 should either show the same profile as Figure 3b in the absence of K8 acetylation, or a combination of traces of both H4K5ac and H4K8ac isomers. Figure 3c exhibits the inverse mobility spectrum of the sum of $b_8^{1+}$, $b_9^{1+}$, $b_{10}^{2+}$ and $b_{11}^{2+}$ ions (black curve), which appears different from Figure 3a. This validates the presence of acetyl group on K8 and by subtracting the contribution of H4K5ac, we thus obtain the inverse mobility distribution of H4K8ac (blue curve).

Figure 3d, shows the b-fragment ion $b_{13}^{2+}$ with an acetyl group (green curve). By comparison with the mobility trace of the sum of H4K5ac and H4K8ac (black curve in Figure 3c), a similar shape is observed, which is explained by the absence of acetylation on K12.

Figure 3e shows inverse mobility distribution of $b_{18}^{3+}$ and $b_{19}^{4+}$ (black curve), which appear to correspond to the sum of contributions of H4K5ac, H4K8ac and H4K16ac. Thus, it is possible to deduce the inverse mobility distribution of H4K16ac (purple curve).

Figure 3f shows, in light green, the sum of the mobility spectra of fragments $b_{24}^{5+}$, $b_{26}^{5+}$, $b_{27}^{3+}$, $b_{28}^{5+}$ and $b_{29}^{4+}$ compared with the precursor distribution (black curve). The similarity between these two curves demonstrates the absence of acetylation of lysines beyond K16.

Finally, we report the estimated inverse mobility distribution of each isomer on Figure 3a (colored lines). These distributions show a very good agreement when compared with TIMS-MS reference spectra measured on individual isomers H4K5ac, H4K8ac and H4K16ac, synthetized in our previous work[32] under same conditions (Figure S4).

In summary, with the combination of TIMS and MS/MS at the intact protein level, we have shown that protein acetyltransferase KAT8 deposits three distinct N-$\varepsilon$-acetylation sites (K16 > K5, K8) on histone H4 as the first degree of acetylation. The three coexisting positional isomers can be separated (as highlighted with dotted lines) allowing the unambiguous assignment of the location of the PTMs thanks to unique MS/MS fragment ions. For each of the highlight peak in Figure 3a, a $R_{IMS}$ of 270, 300 and 288 are calculated for H4K5ac, H4K8ac and H4K16ac, respectively. By manually adjusting the proportion of each contribution (dotted grey line) we can roughly estimate that KAT8 predominantly catalyzes acetylation of K16 with ~50% and K5 and K8 approximately in the same proportion, 30% and 20%, respectively.

Figure 4 focuses on the separation of regioisomers of H4 containing two acetylation marks. Among the different b-ion fragments there is no evidence of additional acetylation sites. Black curve on Figure 4a corresponds to inverse mobility distribution of the precursors which is presumably the cumulative contribution of H4K5acK8ac, H4K5acK16ac and H4K8acK16ac. Figure 4b shows fragments $b_8^{2+}$, $b_9^{2+}$ and $b_{10}^{2+}$ with two acetylation (+84 Da) which can only correspond to H4K5acK8ac. Figure 4c shows the inverse mobility distribution of H4K8acK16ac (cyan), which can be extracted by comparison between fragments $b_{16}^{3+}$, $b_{17}^{3+}$, $b_{19}^{3+}$ with two acetylation corresponding to the sum of H4K5acK8ac, H4K5acK16ac and H4K8acK16ac, and $b_5^{1+}$, $b_6^{1+}$ and $b_7^{1+}$ fragments ions with a single acetylation (grey), which correspond to H4K5acK8ac and H4K5acK16ac isomers. Thus, subtraction of grey curve of to the black one gives the distribution of H4K8acK16ac. Figure 4d shows in purple the distribution of H4K5acK16ac obtained by subtracting the distribution of H4K5acK8ac from the grey distribution of Figure 4c. Lastly, Figure 4e shows the absence of acetylation marks after lysine 16.

Partial separation of each isomer is achieved with the contamination of one isomer in each case, as highlighted with the dotted lines in Figure 4. By reducing the mixture to local binary combinations of isomers and analyzing unique MS/MS fragment, it became possible to estimate the inverse mobility distributions of each diacetylated isomer. Manual adjustment of the sum of these determined distributions (dotted grey line on Figure 4a), to match the precursor

ion distribution, corresponds approximately to proportions of 1:6:3 for H4K5acK8ac, H4K5acK16ac, and H4K8acK16ac, respectively. If the second site of acetylation is independent of the first site, proportions of 2:5:3 would be expected for H4K5acK8ac, H4K5acK16ac, and H4K8acK16ac, respectively, based on the probabilities obtained for monoacetylated species as described above (Figure 3). Hence, the similarity between these proportions suggests that there is no preferred site for the second acetylation and likely no steric hindrance between the closely located K5 and K8 sites. Similar analyses were performed on charge state 17+ displayed on Figures S5 and S6, giving a similar ratio.

Table 1 presents a summary of the CCS centroids for the main contributions of each individual isomer at charge states 16+ and 17+, along with their corresponding resolving power values. All the peaks that have a relative intensity greater than 50% of the maximum amplitude are listed in the table.

## CONCLUSION

We applied trapped IMS separation at the intact protein level for the separation of isomeric proteoforms of post-translationally modified histone H4 decorated produced by enzymatic reaction with acetyltransferase KAT8. We evaluated the catalytic specificity of KAT8 and estimated a reaction yield of approximately 80% after 3 hours. The reaction resulted in mono-, di-, and tri-acetylation products, with singly acetylated histone constituting half of the total acetylated H4 produced (Figure 2). We successfully characterized KAT8 specificity and validated its preference for acetylation at K16 site. Additionally, we have identified the existence of acetylation at K5 and K8 already at the first degree of acetylation. Our findings corroborate the recent reports on protein complex dependent substrate specificity of KAT8 for acetylation of histone H4[34]. We demonstrated that the KAT8 enzyme has inherent and promiscuous in vitro substrate specificity for K5, K8 and K16 of histone H4. This activity is likely fine-tuned by protein factors in chromatin binding complexes in vivo.

By maximizing the resolving power of the instrument, we fully separated these three regioisomers (H4K5ac, H4K8ac and H4K16ac) at charge state 16+, achieving $R_{IMS}$ values up to 300 (Figure 3). In absence of efficient separation methods, relying solely on MS/MS to handle more than two isomers leads to chimeric spectra due to shared characteristic fragment ions between H4K5ac/H4K8ac and H4K8ac/H4K16ac pairs, prohibiting the identification of H4K8ac. More generally, this limitation impedes the quantification and the discovery of

unknown proteoforms or PTMs that may be present. TIMS-MS/MS(CID) demonstrates its ability to perform enzymatic assays as the protein level and precisely identify proteoforms and sites of PTMs.

The detection of unique fragment ions not only validates the fully TIMS-separated species without requiring reference compounds, but also enable the estimation of mobility distributions of partially/unseparated species, thanks to the reduction of the spectra complexity induced by IMS. This was demonstrated by the partial separation of the three PTM positional isomers, which presents two nearby acetylation sites each (H4K5acK8ac, H4K5acK16ac and H4K8acK16ac) (Figure 4). The achieved separation was sufficient to estimate their mobility distribution. The resulting CCS values and CCS distribution shapes can serve as reference spectra for future investigations and as benchmarks for theoretical calculation of protein structure[41]. In addition, the reduction of MS/MS spectral complexity induced by IMS could allow for assignment of internal fragments, which can extend protein sequence coverage[42].

These results open new possibilities for further exploratory and systematic top-down studies of PTMs using IMS in biological samples that have a higher degree of complexity, which presents several challenges. A higher resolution and/or separation capability is needed to separate high number of potential proteoforms, and since IMS is orthogonal to chromatographic separation, it offers a compatible duty cycle for 2D IMS-LC separation[23]. LC can be used as separation and purification step prior IMS separation to fractionate sample, and in the case of histone proteins may assess the acetylation and methylation degrees[43,20]. Furthermore, an more efficient methods for intact protein sequencing is needed. CID produces spectra with a more limited peptide backbone fragmentation than electron capture or transfer based dissociation (ExD), which generate more complete series of ions. As a result, ExD provides more extensive sequence information, enabling a more accurate identification of PTM sites, while also preserving labile PTMs[44]. Recent technological developments of new hybrid electrostatic/magnetostatic cells has enabled the coupling of ECD with time-of-flight mass analyzer[45,46]. Additionally, the development of multidimensional and multiple-stage MS/MS techniques[47] holds significant potential for intact protein analysis, and permits automatic and systemic investigation of fragment conditions to maximize amino acid sequence coverage.[48] These advancements offer great prospects for expanding top-down IMS-MS/MS applications.

**Conflicts of interest statement:** The authors declare no conflict of interest.

# REFERENCES

[1] Spoel, S.H., Orchestrating the proteome with post-translational modifications. *J Exp Bot* 2018, 69, 4499–4503.

[2] Wang, Y.-C., Peterson, S.E., Loring, J.F., Protein post-translational modifications and regulation of pluripotency in human stem cells. *Cell Res* 2014, 24, 143–160.

[3] Vasudevan, V., Agnihotri, P., Biswas, S., Post Translational Modification and Its Pathologic Association in Rheumatoid Arthritis: A Brief Perspective. *Curr Protein Pept Sci* 2021, 22, 548–558.

[4] Pan, S., Chen, R., Pathological implication of protein post-translational modifications in cancer. *Mol Aspects Med* 2022, 86, 101097.

[5] Meng, F., Liang, Z., Zhao, K., Luo, C., Drug design targeting active posttranslational modification protein isoforms. *Medicinal Research Reviews* 2021, 41, 1701–1750.

[6] Proietti, G., Wang, Y., Punzo, C., Mecinović, J., Substrate Scope for Human Histone Lysine Acetyltransferase KAT8. *Int J Mol Sci* 2021, 22, 846.

[7] Jenuwein, T., Allis, C.D., Translating the Histone Code. *Science* 2001, 293, 1074–1080.

[8] Smith, B.J., Carregari, V.C., Histone Modifications in Neurological Disorders. *Adv Exp Med Biol* 2022, 1382, 95–107.

[9] Neganova, M.E., Klochkov, S.G., Aleksandrova, Y.R., Aliev, G., Histone modifications in epigenetic regulation of cancer: Perspectives and achieved progress. *Seminars in Cancer Biology* 2022, 83, 452–471.

[10] Keenan, E.K., Zachman, D.K., Hirschey, M.D., Discovering the landscape of protein modifications. *Molecular Cell* 2021, 81, 1868–1878.

[11] Ivry, S.L., Meyer, N.O., Winter, M.B., Bohn, M.F., et al., Global substrate specificity profiling of post-translational modifying enzymes. *Protein Sci* 2018, 27, 584–594.

[12] Smith, L.M., Kelleher, N.L., Proteoforms as the next proteomics currency. *Science* 2018, 359, 1106–1107.

[13] Koch, C.M., Andrews, R.M., Flicek, P., Dillon, S.C., et al., The landscape of histone modifications across 1% of the human genome in five human cell lines. *Genome Res.* 2007, 17, 691–707.

[14] Kaimori, J.-Y., Maehara, K., Hayashi-Takanaka, Y., Harada, A., et al., Histone H4 lysine 20 acetylation is associated with gene repression in human cells. *Sci Rep* 2016, 6, 24318.

[15] Barski, A., Cuddapah, S., Cui, K., Roh, T.-Y., et al., High-Resolution Profiling of Histone Methylations in the Human Genome. *Cell* 2007, 129, 823–837.

[16] Smith, L.E., Rogowska-Wrzesinska, A., The challenge of detecting modifications on proteins. *Essays in Biochemistry* 2020, 64, 135–153.

[17] Brown, K.A., Melby, J.A., Roberts, D.S., Ge, Y., Top-down proteomics: challenges, innovations, and applications in basic and clinical research. *Expert Rev Proteomics* 2020, 17, 719–733.

[18] Siuti, N., Kelleher, N.L., Decoding protein modifications using top-down mass spectrometry. *Nat Methods* 2007, 4, 817–821.

[19] El Kennani, S., Crespo, M., Govin, J., Pflieger, D., Proteomic Analysis of Histone Variants and Their PTMs: Strategies and Pitfalls. *Proteomes* 2018, 6, 29.

[20] Holt, M.V., Wang, T., Young, N.L., High-Throughput Quantitative Top-Down Proteomics: Histone H4. *J. Am. Soc. Mass Spectrom.* 2019, 30, 2548–2560.

[21] A. Graham, K., F. Lawlor, C., B. Borotto, N., Characterizing the top-down sequencing of protein ions prior to mobility separation in a timsTOF. *Analyst* 2023, 148, 1534–1542.

[22]    Zinnel, N.F., Pai, P.-J., Russell, D.H., Ion Mobility-Mass Spectrometry (IM-MS) for Top-Down Proteomics: Increased Dynamic Range Affords Increased Sequence Coverage. *Anal. Chem.* 2012, 84, 3390–3397.

[23]    D'Atri, V., Causon, T., Hernandez-Alba, O., Mutabazi, A., et al., Adding a new separation dimension to MS and LC-MS: What is the utility of ion mobility spectrometry? *J Sep Sci* 2018, 41, 20–67.

[24]    Dodds, J.N., Baker, E.S., Ion Mobility Spectrometry: Fundamental Concepts, Instrumentation, Applications, and the Road Ahead. *J Am Soc Mass Spectrom* 2019, 30, 2185–2195.

[25]    Christofi, E., Barran, P., Ion Mobility Mass Spectrometry (IM-MS) for Structural Biology: Insights Gained by Measuring Mass, Charge, and Collision Cross Section. *Chem. Rev.* 2023, 123, 2902–2949.

[26]    Kirk, A.T., Bohnhorst, A., Raddatz, C.-R., Allers, M., Zimmermann, S., Ultra-high-resolution ion mobility spectrometry—current instrumentation, limitations, and future developments. *Anal Bioanal Chem* 2019, 411, 6229–6246.

[27]    Michelmann, K., Silveira, J.A., Ridgeway, M.E., Park, M.A., Fundamentals of Trapped Ion Mobility Spectrometry. *J. Am. Soc. Mass Spectrom.* 2015, 26, 14–24.

[28]    Giles, K., Ujma, J., Wildgoose, J., Pringle, S., et al., A Cyclic Ion Mobility-Mass Spectrometry System. *Anal. Chem.* 2019, 91, 8564–8573.

[29]    Ibrahim, Y.M., Hamid, A.M., Deng, L., Garimella, S.V.B., et al., New frontiers for mass spectrometry based upon structures for lossless ion manipulations. *Analyst* 2017, 142, 1010–1021.

[30]    Hollerbach, A.L., Li, A., Prabhakaran, A., Nagy, G., et al., Ultra-High-Resolution Ion Mobility Separations Over Extended Path Lengths and Mobility Ranges Achieved using a Multilevel Structures for Lossless Ion Manipulations Module. *Anal. Chem.* 2020, 92, 7972–7979.

[31]    Garabedian, A., Baird, M.A., Porter, J., Jeanne Dit Fouque, K., et al., Linear and Differential Ion Mobility Separations of Middle-Down Proteoforms. *Anal. Chem.* 2018, 90, 2918–2925.

[32]    Berthias, F., Thurman, H.A., Wijegunawardena, G., Wu, H., et al., Top-Down Ion Mobility Separations of Isomeric Proteoforms. *Anal. Chem.* 2023, 95, 784–791.

[33]    Shia, W.-J., Pattenden, S.G., Workman, J.L., Histone H4 lysine 16 acetylation breaks the genome's silence. *Genome Biol* 2006, 7, 217.

[34]    Radzisheuskaya, A., Shliaha, P.V., Grinev, V.V., Shlyueva, D., et al., Complex-dependent histone acetyltransferase activity of KAT8 determines its role in transcription and cellular homeostasis. *Molecular Cell* 2021, 81, 1749-1765.e8.

[35]    Proietti, G., Rainone, G., Hintzen, J.C.J., Mecinović, J., Exploring the Histone Acylome through Incorporation of γ-Thialysine on Histone Tails. *Bioconjug Chem* 2020, 31, 844–851.

[36]    Simon, M.D., Chu, F., Racki, L.R., de la Cruz, C.C., et al., The Site-Specific Installation of Methyl-Lysine Analogs into Recombinant Histones. *Cell* 2007, 128, 1003–1012.

[37]    Fernandez-Lima, F.A., Kaplan, D.A., Park, M.A., Note: Integration of trapped ion mobility spectrometry with mass spectrometry. *Review of Scientific Instruments* 2011, 82, 126106.

[38]    Hernandez, D.R., DeBord, J.D., Ridgeway, M.E., Kaplan, D.A., et al., Ion dynamics in a trapped ion mobility spectrometer. *Analyst* 2014, 139, 1913–1921.

[39]    Ridgeway, M.E., Lubeck, M., Jordens, J., Mann, M., Park, M.A., Trapped ion mobility spectrometry: A short review. *International Journal of Mass Spectrometry* 2018, 425, 22–35.

[40]    Marty, M.T., Baldwin, A.J., Marklund, E.G., Hochberg, G.K.A., et al., Bayesian Deconvolution of Mass and Ion Mobility Spectra: From Binary Interactions to Polydisperse Ensembles. *Anal. Chem.* 2015, 87, 4370–4376.

[41]    Lee, J.W., Davidson, K.L., Bush, M.F., Kim, H.I., Collision cross sections and ion structures: development of a general calculation method via high-quality ion mobility measurements and theoretical modeling. *Analyst* 2017, 142, 4289–4298.

[42]    Zenaidee, M.A., Wei, B., Lantz, C., Wu, H.T., et al., Internal Fragments Generated from Different Top-Down Mass Spectrometry Fragmentation Methods Extend Protein Sequence Coverage. *J. Am. Soc. Mass Spectrom.* 2021, 32, 1752–1758.

[43]    Molden, R.C., Garcia, B.A., Middle-down and Top-down mass spectrometric analysis of co-occurring histone modifications. *Curr Protoc Protein Sci* 2014, 77, 23.7.1-23.7.28.

[44]    Brodbelt, J.S., Ion Activation Methods for Peptides and Proteins. *Anal. Chem.* 2016, 88, 30–51.

[45]    Voinov, V.G., Deinzer, M.L., Barofsky, D.F., Radio-Frequency-Free Cell for Electron Capture Dissociation in Tandem Mass Spectrometry. *Anal Chem* 2009, 81, 1238–1243.

[46]    Beckman, J.S., Voinov, V.G., Hare, M., Sturgeon, D., et al., Improved Protein and PTM Characterization with a Practical Electron-Based Fragmentation on Q-TOF Instruments. *J Am Soc Mass Spectrom* 2021, 32, 2081–2091.

[47]    Papanastasiou, D., Kounadis, D., Lekkas, A., Orfanopoulos, I., et al., The Omnitrap Platform: A Versatile Segmented Linear Ion Trap for Multidimensional Multiple-Stage Tandem Mass Spectrometry. *J. Am. Soc. Mass Spectrom.* 2022, 33, 1990–2007.

[48]    Shliaha, P.V., Gibb, S., Gorshkov, V., Jespersen, M.S., et al., Maximizing Sequence Coverage in Top-Down Proteomics By Automated Multimodal Gas-Phase Protein Fragmentation. *Anal Chem* 2018, 90, 12519–12526.
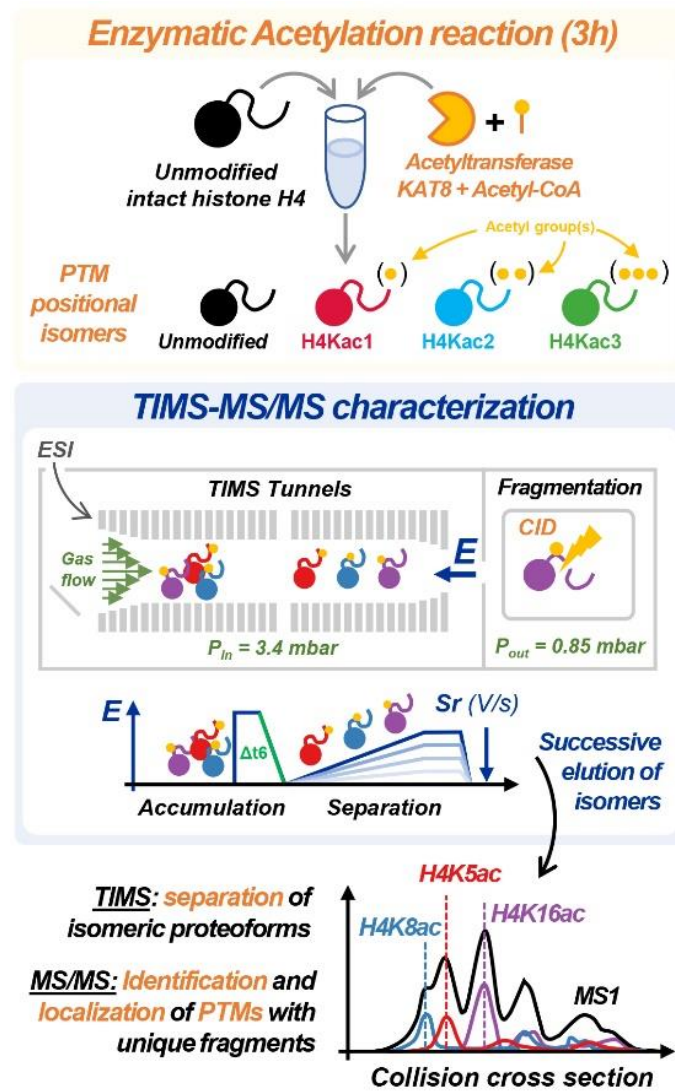
Figure 1. Schematic overview of the top-down TIMS-MS/MS(CID) characterization of isomeric proteoforms of generated by enzymatic reaction.
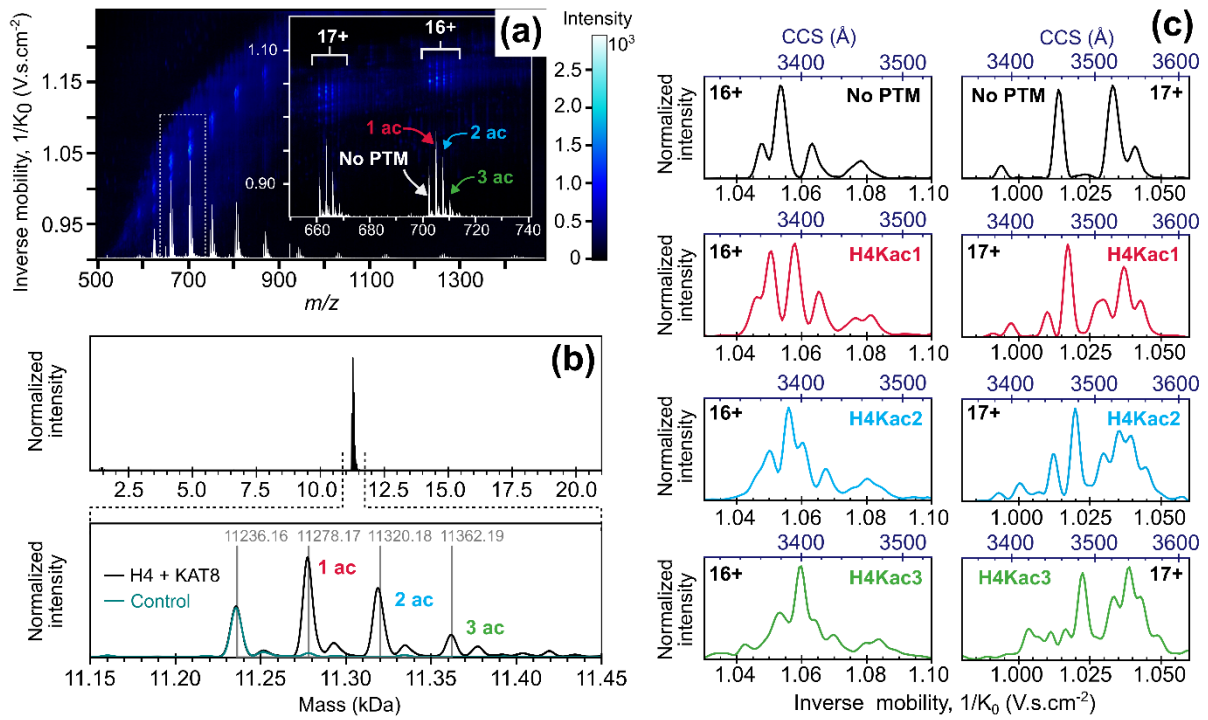
Figure 2: Evaluation of KAT8 enzyme activity on histone H4 after 3 hours of incubation. (a) Heatmap showing inverse mobility as a function of mass-over-charge ratio. (b) Deconvoluted mass spectra of H4 with KAT8 (black) and control (teal) samples, along with theoretical average mass of unmodified and acetylated H4. Each peak exhibits an additional feature with a mass difference of +16 Da is observed for each peak, possibly indicating the oxidation of the unique methionine residue (M84). (c) TIMS-MS spectra for unmodified and acetylated H4 for charge state 16+ and 17+ at a scan rate value of 23 V/s.

# H4Kac1

$\overleftarrow{S}$ G R G K G G K G L G K G G A K R H R K$^{20}$
V L R D N I Q G I T K P A I R R L A R R$^{40}$
G G V K R I S G L I Y E E T R G V L K V$^{60}$
F L E N V I R D A V T Y T E H A K R K T$^{80}$
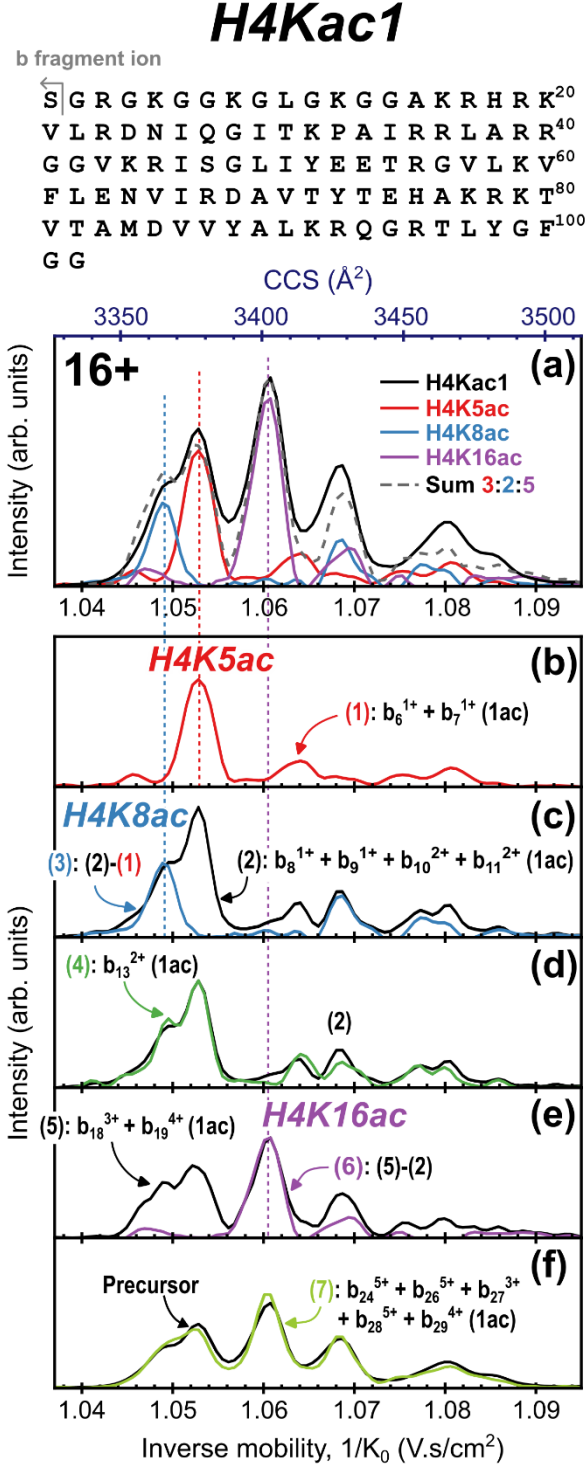V T A M D V V Y A L K R Q G R T L Y G F$^{100}$
G G



Figure 3: Separation and identification of isomeric proteoforms of monoacetylated H4 (H4ac1) produced by acetyltransferase reaction with KAT8 at charge states 16+. (a) TIMS spectra of the precursor ion (black) and identified individual isomer (colors). (b)-(f) TIMS-MS/MS(CID) spectra of characteristic b fragment ions allowing the identification of the acetylated lysine.
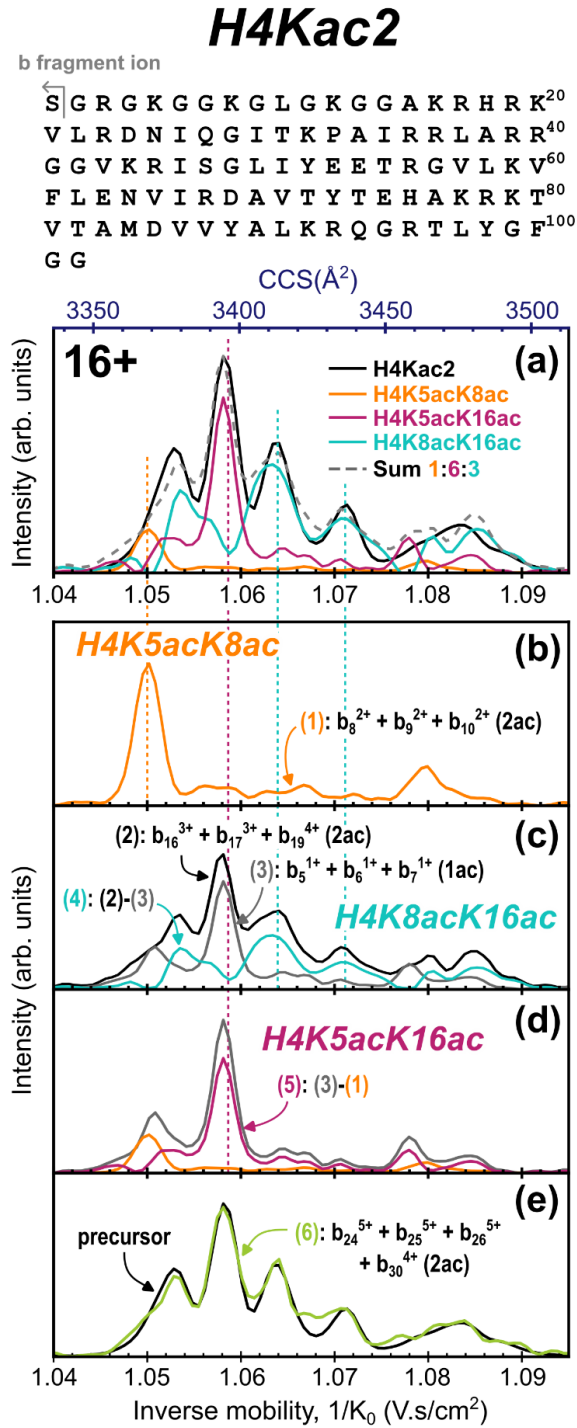
Figure 4: Separation and identification of isomeric proteoforms of diacetylated H4 (H4ac2) produced by acetyltransferase reaction with KAT8 at charge states 16+. (a) TIMS spectra of the precursor ion (black) and identified individual isomer (colors). (b)-(e) TIMS-MS/MS(CID) spectra of characteristic b fragment ions allowing the identification of the acetylated lysine residues.

Table 1: Summary table of the inverse mobility distributions of each isomer for mono- and diacetylated species at charge states 16+ and 17+.

| z | Proteoform | $<1/K_0>$ (Vs/cm$^2$) | CCS (A$^2$) | R |
|---|---|---|---|---|
| 16+ | H4K5ac | 1.053 | 3378 | 270 |
| | H4K8ac | 1.049 | 3365 | 301 |
| | H4K16ac | 1.061 | 3400 | 288 |
| | H4K5acK8ac | 1.050 | 3369 | 309 |
| | H4K5acK16ac | 1.058 | 3394 | 369 |
| | H4K8acK16ac | 1.063 | 3412 | 218 |
| | | 1.071 | 3436 | 225 |
| 17+ | H4K5ac | 1.011 | 3447 | 306 |
| | | 1.033 | 3520 | 187 |
| | H4K8ac | 1.017 | 3468 | 239 |
| | | 1.029 | 3509 | 294 |
| | H4K16ac | 1.018 | 3469 | 285 |
| | | 1.038 | 3539 | 210 |
| | H4K5acK8ac | 1.030 | 3304 | 192 |
| | H4K5acK16ac | 1.013 | 3252 | 224 |
| | | 1.037 | 3328 | 164 |
| | H4K8acK16ac | 1.020 | 3271 | 268 |